Journal of Solid Mechanics Vol. 16, No. 1 (2024) pp. 74-96

Research Paper

The Nonlinear Thermo-Hyperelastic Analysis of Functionally Graded Incompressible Hollow Sphere with Temperature Dependent Material Using Finite Element Method

A. Zargaripoor [*] , M. Shariyat

Faculty of Mechanical Engineering, K.N. Toosi University of Technology, Tehran 19991-43344, Iran

Received 8 May 2024; Received in revised form 26 June 2024; Accepted 2 July 2024

ABSTRACT

In this research, a nonlinear finite element formulation is investigated for analysis of the stress, displacement, and temperature distributions of thermo hyperelastic hollow spheres subjected to mechanical and thermal forces. It is assumed that the hollow sphere is made of functionally graded and temperature-dependent material. By considering the concept of multiplicative decomposition of the deformation gradient, the coupled nonlinear equations are derived. Mechanical and thermal parts are considered for studying the thermo-hyperelastic behavior. The governing equations are found by considering the incompressible Mooney-Rivlin hyperelastic model. Distribution of displacement, stress components, and temperature through the thickness of the hollow sphere are plotted for different constitutive, temperature dependency, and inhomogeneity parameters. The obtained results indicate that the temperature dependency of the material and inhomogeneity properties have a significant influence on displacement, stress components, and temperature distribution along the radial direction.

Keywords: Hyperelastic; Functionally graded material; Temperature dependent material.

1 INTRODUCTION

IN hyper-elastic materials the reaction to the stresses is not proportional to the strain. So, it is important to find a suitable relation between stress and strain in hyperelastic materials to analysis of their nonlinear responses The link between stress and strain in these materials is obtained from a strain energy function. So, some hyperelastic

[*]Corresponding author.
E-mail address: Alizargaripoor@email.kntu.ac.ir

theoretical models such as Neo-Hookean [1], Mooney-Rivlin [2], and Ogden [3] have been developed to capture the stress-strain response of large deformation. The strain energy function in Mooney-Rivlin and neo-Hookean models is composed from invariants of the left Cauchy-Green deformation tensor. While, the stress energy function in Ogden model is defined by the principal stretch ratio.

Many researchers employed hyperelastic models to study thick-walled cylinders and spheres under various boundary conditions. These structures have many industrial applications such as pipes, cooling towers, and liquid storage tanks. So, it is an interesting aren to investigation for mechanical engineering.

Taghizadeh et al.[4] presented some research about cylindrical tubes and spherical shells that composed of hyperelastic materials and soft tissues. Aranda-Iglesias et al. [5] presented forced and free nonlinear radial oscillations of a thick-walled cylindrical shell. Breslavsky et al. [6] presented dynamic and static responses of a cylindrical shell composed of rubber-like materials. Anani and Rahimi [7] used the theory of hyperelasticity to analyze the rotating thick-walled hollow cylindrical shells that made of functionally graded material. A.Ghorbanpour Arani et al. [8] investigated vibration and instability of visco-elasticity coupled carbon nanotube reinforced composite microtubes conveying fluid. A.H, Ghorbanpour Arani et al. [9] presented the analysis of free and forced vibrations of double viscoelastic piezoelectric nanobeam systems incorporating nonlocal viscoelasticity theory and Euler-Bernoulli beam model.A.Ghorbanpour Arani et al. [10] extended the original formulation of the quasi-3D sinusoidal shear deformation plate theory to the wave propagation analysis of viscoelastic sandwich nanoplates considering surface effects. A.H.Ghorbanpour et al. [11] presented analysis of the size-dependent wave propagation of coupled double-walled boron nitride nanotubes conveying nanoflow systems based on Timoshenko beam theory. Narooei and Arman [12] offered the unstressed initial configuration by using the exponential stretched-based hyperelastic strain energy. Ataee and Noroozi [13] illustrated an optimization problem for different stretch ratios and geometries in the biaxial loading of the membrane. Gharooni and Ghannad [14] worked on thick-walled cylindrical shell that composed of rubber-like materials to present a nonlinear analytical solution. In another research, they worked on functionally graded cylindrical pressure vessels in the nearly incompressible state under non-uniform pressure loading [15]. Anani and Rahimi [16] worked on functionally graded thick-wall hyperelastic cylindrical and spherical shells that subjected to internal pressure. Shariyat et al. [17] presented the displacement and stress distribution of hyperelastic cylindrical vessels that subjected to internal pressure. Zhao et al. [18] presented the dynamic responces of spherical shell made of visco-hyperelastic materials subjected to radial loads. A.H. Ghorbanpour-Arani et al. [19] investigated nonlinear dynamic analysis of an embedded functionally graded sandwich nanobeam integrated with magnetostrictive layers. Haghparast et al. [20] presented theoretical investigation to analyze vibration of axially moving sandwich plate floating on fluid. Benslimane [21] studied an incompressible isotriopic nonlinear elastic thick walled spherical structure subjected to internal pressure using analytical formulation. Jemiolo and Franus [22] used finite element method to present a study on a hyperelastic cylindrical tube. Aghaienezhad et al. [23] analyse the behaviour of cylindrical and spherical shell by driving the incremental equilibrium equations.They assumed that the shells are subjected to external pressure. Anssari-Benam et al. [24] worked on incompressible hyperelastic cylindrical and spherical shells by propsing a generalized neo-Hookean model. A.A.Ghorbanpour Arani et al. [25] investigated response of a smart sandwich plate made of magnetic face sheets and reinforced core with nano-fibers.A. Ghorbanpour Arani et al. [26] investigated the recent developments in the field of non-intrinsic repair systems with an emphasis on their use in polymer composites. Sourani et al. [27] analysed the nonlinear dynamic stability of carbon nanotube reinforced composite piezoelectric viscoelastic nano/micro plate under time dependent harmonic compressive biaxial mechanical loading.

In many cases, hyperelastic materials are exposed to finite deformations combined with temperature changes. By decomposing the deformation gradient tensor into a mechanical and thermal part, a suitable model for this material can be obtained. Recently, many studies have analyzed the thermo-hyperelastic problems.

Yosibash et al. [28] used finite element method to analyse the thermo-hyperelastic system by considering the temperature dependency of the materials. Almasi et al. [29] analysed the hyperelastic cylindrical pressure using multiplicative decomposition of the deformation gradient tensor both numerically and analytically. Xu et al. [30] studied an incompressible thermo-hyperelastic cylinder that subjected to an axial load at its ends. Also, they considered a temperature field at its lateral boundary. In another work, they used the third-order shear deformation theory to study the vibration of hyperelastic thick cylindrical shell an a temperature filed. [31]. Mirparizi and fotuhi [32] studied the wave reflection and propagation in a nearly incompressible thermo-hyperelastic finite-length solid using nonlinear finite element formulation. Shakeriski et al. [33] studied stress and thermal wave propagation in a near incompressible medium using generalized thermo-hyperelastic model. Wang et al. [34] adopted the constitutive relation of slightly nonlinear traveling waves in a thermo-hyperelastic cylindrical shell. Bakhtiyari et al. [35] modified the constitutive model for shape memory polymers based on the concept of internal state variables and rational thermodynamics in large deformation. Mohammadlou et al. [36] presented the thermal stresses and strains

in a thin-walled conical shell subjected to uniform heat flow along its side surfaces and at both ends of the thermal insulation shell.

In this paper, we present a nonlinear finite element formulation for analysis of the stress, displacement, and temperature distributions of thermo- hyperelastic hollow spheres subjected to mechanical and thermal forces. This is significant because the sphere is made of temperature dependent material and this makes the problem more complicated to analyze. According to present literature review, there are some papers based on hyperelastic materials but there is no research about thermo-hyperelastic behavior of temperature dependent materials.

In this paper, a nonlinear finite element formulation based on Mooney-Rivlin hyperelastic model is derived, then the influence of temperature dependency and heterogeneity of the materials is considered.

2 PROBLEM FORMULATION

2.1. Governing Equation

Figure 1 shows a thermo-hyperelastic hollow sphere composed of incompressible, functionally graded, and temperature-dependent material with an inner radius of A and an outer radius of B. (r,ϑ,ϕ) is a spherical coordinate in the deformed configuration and (R,Θ,Φ) is the undeformed one. So, the deformation field is described as follows

$$r = r(R)\ ,\ \vartheta=\Theta\ ,\ \phi=\Phi$$
$$A \le R \le B \tag{1}$$

Here, it is presumed that the hollow sphere is made of functionally graded material, and the materials are temperature dependent. So, variations of a typical material property P may be related to the inner layer, as follows:

$$P(R,T) = P_0 f(T)(\frac{R}{A})^m \tag{2}$$

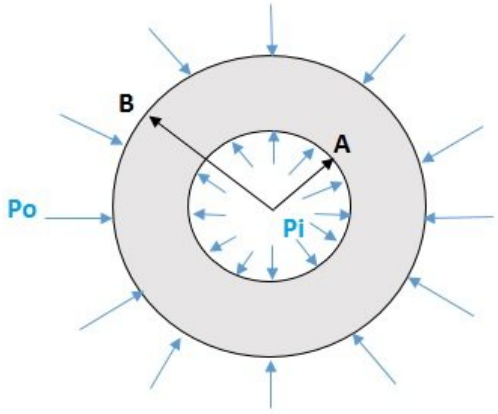

Fig. 1
The schematic of FG thermo-hyperelastic hollow.

where P is the material properties of the hollow sphere such as hyperelastic parameters C_{10}, C_{01} and thermal conductivity (K). P_0 is the value of the mentioned property at the inner layer. Also, $f(T)$ is a linear function of temperature and the positive definite power (m) is the so-called inhomogeneity parameter. The linear function of temperature ($f(T)$) is defined as follows

$$f(R,T) = 1 + a\frac{T(R)}{T_0} \tag{3}$$

where a is constant.
In spherical coordinates, the deformation gradient tensor is described as follows [21]

$$[F] = \begin{bmatrix} \dfrac{\partial r}{\partial R} & \dfrac{1}{R}\dfrac{\partial r}{\partial \Theta} & \dfrac{1}{R\sin\Theta}\dfrac{\partial r}{\partial \Phi} \\ r\dfrac{\partial \vartheta}{\partial R} & \dfrac{r}{R}\dfrac{\partial \vartheta}{\partial \Theta} & \dfrac{r}{R\sin\Theta}\dfrac{\partial \vartheta}{\partial \Phi} \\ r\sin\vartheta\dfrac{\partial \phi}{\partial R} & \dfrac{r\sin\vartheta}{R}\dfrac{\partial \phi}{\partial \Theta} & \dfrac{r\sin\vartheta}{R\sin\Theta}\dfrac{\partial \phi}{\partial \Phi} \end{bmatrix} \tag{4}$$

For one-dimensional problems and by considering the symmetry of the hollow sphere, Eq. (4) may be rewritten as follows [21]

$$[F] = \begin{bmatrix} \dfrac{\partial r}{\partial R} & 0 & 0 \\ 0 & \dfrac{r}{R} & 0 \\ 0 & 0 & \dfrac{r}{R} \end{bmatrix} \rightarrow J = \det(F) \tag{5}$$

The multiplicative decomposition of the deformation gradient into a mechanical part F_M and thermal part F_T and is considered.[37]

$$F = F_T F_M \quad , J = J_T J_M \tag{6}$$

The thermal part F_T can be described as follows [37]

$$F_T = \varphi(R,T) I \tag{7}$$

$$\varphi(R,T) = 1 + \alpha(T(R) - T_0) \tag{8}$$

Where $\varphi(R,T)$ is a function of temperature and radial of sphere and α is the thermal expansion coefficient. For incompressible material $J_M = 1$ and for the total volume change J we have

$$J_M = 1 \rightarrow J = J_T = \varphi^3(R,T) \tag{9}$$

Also, we know

$$U = r - R \quad \text{or} \quad r = U + R \tag{10}$$

So, the gradient deformation tensor of Eq. (5) can be rewritten as follows

$$[F] = \begin{bmatrix} 1+\dfrac{\partial U}{\partial R} & 0 & 0 \\ 0 & 1+\dfrac{U}{R} & 0 \\ 0 & 0 & 1+\dfrac{U}{R} \end{bmatrix} \tag{11}$$

Also, the right Cauchy-Green tensor and the Green strain tensor are

$$[C] = F^T F = \begin{bmatrix} (1+\dfrac{\partial U}{\partial R})^2 & 0 & 0 \\ 0 & (1+\dfrac{U}{R})^2 & 0 \\ 0 & 0 & (1+\dfrac{U}{R})^2 \end{bmatrix} \tag{12}$$

$$[E] = \begin{bmatrix} \dfrac{1}{2}(\dfrac{\partial U}{\partial R})^2 + \dfrac{\partial U}{\partial R} & 0 & 0 \\ 0 & \dfrac{1}{2}(\dfrac{U}{R})^2 + \dfrac{U}{R} & 0 \\ 0 & 0 & \dfrac{1}{2}(\dfrac{U}{R})^2 + \dfrac{U}{R} \end{bmatrix} \tag{13}$$

By using Eq. (6) we have

$$C_M = \varphi^{-2}(R,T)C \tag{14}$$

$$I_{C_M} = \varphi^{-2}(R,T)I_C \tag{15}$$

$$II_{C_M} = \varphi^{-4}(R,T)II_C \tag{16}$$

$$III_{C_M} = \varphi^{-6}(R,T)III_C \tag{17}$$

The second Piola-Kirchhoff stress for a hyperelastic material will be obtained from a free energy function $\psi(C,T)$ as follows [38]:

$$\gamma = 2\rho\frac{\partial\psi(C,T)}{\partial C} \tag{18}$$

In an isothermal deformation, a strain energy function describe the free energy function. While, in a non-isothermal deformation, a strain energy function couled be used instead of the free energy function by considering the thermal changes and mechanical deformation [38].

$$\psi(C,T) = W(C_M,T) + W(T) \tag{19}$$

where $W(C_M,T)$ is the strain energy function which depends on mechanical deformation and $W(T)$ is an arbitrary function of temperature.

So, for Eq. (18) we have:

$$\gamma = 2\rho\frac{\partial\psi(C,T)}{\partial C} = 2\rho\frac{\partial W(C_M,T)}{\partial C} \tag{20}$$

Applying the chain rule to Eq. (20) yields

$$\frac{\partial W(C_M,T)}{\partial C} = \frac{\partial W(C_M,T)}{\partial C_M}\frac{\partial C_M}{\partial C} = \varphi^{-2}(R,T)\frac{\partial W(C_M,T)}{\partial C_M} \tag{21}$$

$$\gamma = 2\rho\varphi^{-2}(R,T)\frac{\partial W(C_M,T)}{\partial C_M} \tag{22}$$

The Cauchy stress tensor could be derived from Eq. (22)

$$\sigma = \frac{1}{J}F^T\gamma F \tag{23}$$

$$\sigma = \frac{1}{\varphi^3(T)}F^T(2\rho\varphi^{-2}(R,T)\frac{\partial W(C_M,T)}{\partial C_M})F \tag{24}$$

By applying the chain rule we have

$$\frac{\partial W(C_M,T)}{\partial C_M} = \frac{\partial W(C_M,T)}{\partial I_{C_M}}\frac{\partial I_{C_M}}{\partial C_M} + \frac{\partial W(C_M,T)}{\partial II_{C_M}}\frac{\partial II_{C_M}}{\partial C_M} \tag{25}$$

For derivatives of Eq. (25) we have [39]:

$$\frac{\partial I_{C_M}}{\partial C_M} = \frac{\partial I_C}{\partial C} = I \tag{26}$$

$$\begin{aligned} &\frac{\partial II_C}{\partial C} = I_C I - C \\ &\frac{\partial II_{C_M}}{\partial C_M} = \frac{\partial II_{C_M}}{\partial C}\frac{\partial C}{\partial C_M} = \varphi^2(R,T)\frac{\partial II_{C_M}}{\partial C} = \varphi^2(R,T)\varphi^{-4}(R,T)\frac{\partial II_C}{\partial C} = \varphi^{-2}(R,T)(I_C I - C) \end{aligned} \tag{27}$$

So, the Cauchy stress tensor could be derived by considering Eqs. (24-27) [38]

$$\sigma = \frac{2\rho}{\varphi^7(R,T)} F^T((\varphi^2(R,T)\frac{\partial W(C_M,T)}{\partial I_{C_M}} I + \frac{\partial W(C_M,T)}{\partial II_{C_M}}(I_C I - C)))F - pI \tag{28}$$

2.2. Mooney-Rivlin Model:

The strain energy function for incompressible and temperature-dependent material and functionally graded Mooney-Rivlin model can be described as follows [40]:

$$\rho W(C_M,T) = C_{10}(R,T)(I_{C_M} - 3) + C_{01}(R,T)(II_{C_M} - 3) \tag{29}$$

The components of the Cauchy stress tensor could be derived from Eqs. (28-29)

$$\sigma_R = \frac{2\rho}{\varphi^7(R,T)}\left[\frac{C_{10}}{\rho}\varphi^2(R,T)(1+\frac{\partial U}{\partial R})^2 + \frac{2C_{01}}{\rho}(1+\frac{\partial U}{\partial R})^2(1+\frac{U}{R})^2\right] - p \tag{30}$$

$$\sigma_\theta = \frac{2\rho}{\varphi^7(R,T)}\left[\frac{C_{10}}{\rho}\varphi^2(R,T)(1+\frac{U}{R})^2 + \frac{C_{01}}{\rho}(1+\frac{U}{R})^2((1+\frac{\partial U}{\partial R})^2 + (1+\frac{U}{R})^2)\right] - p \tag{31}$$

In the absence of body force, the equilibrium equation in the radial direction is described as:

$$\frac{d\sigma_R}{dR} + \frac{2(\sigma_R - \sigma_\vartheta)}{R} = 0 \tag{32}$$

Subsitituting σ_R and σ_θ from Eqs. (30-31) into Eq. (32), the governing equation of motion could be rewritten as:

$$\psi_1\frac{\partial^2 U}{\partial R^2} + \psi_2\frac{\partial U}{\partial R} + \psi_3\frac{\partial T}{\partial R} + \psi_4 U + \psi_5 = 0 \tag{33}$$

where

$$\psi_1 = \frac{4C_{10}R^m}{A^m\varphi^5(R,T)} f(R,T)(1+\frac{\partial u}{\partial R}) + \frac{8C_{01}R^m}{A^m\varphi^7(R,T)} f(R,T)(1+\frac{\partial u}{\partial R})(1+\frac{u}{R})^2 \tag{34}$$

$$\psi_2 = \frac{8C_{01}R^{m-1}}{A^m\varphi^7(R,T)} f(R,T)(1+\frac{\partial u}{\partial R})^2(1+\frac{u}{R}) \tag{35}$$

$$\begin{aligned}\psi_3 = &\frac{2C_{10}aR^m}{A^m\varphi^5(R,T)T_0}(1+\frac{\partial u}{\partial R})^2 - \frac{10C_{10}R^{2m}\alpha_0}{A^{2m}\varphi^6(R,T)} f(R,T)(1+\frac{\partial u}{\partial R})^2 \\ &+\frac{4C_{01}aR^m}{A^m\varphi^7(R,T)T_0}(1+\frac{\partial u}{\partial R})^2(1+\frac{u}{R})^2 - \frac{28C_{01}R^{2m}\alpha_0}{A^{2m}\varphi^8(R,T)} f(R,T)(1+\frac{\partial u}{\partial R})^2(1+\frac{u}{R})^2\end{aligned} \tag{36}$$

$$\psi_4 = -\frac{8C_{01}R^{m-2}}{A^m\varphi^7(R,T)} f(R,T)(1+\frac{\partial u}{\partial R})^2(1+\frac{u}{R}) \tag{37}$$

$$\begin{aligned}\psi_5 = &\frac{2mC_{10}R^{m-1}}{A^m\varphi^5(R,T)} f(R,T)(1+\frac{\partial U}{\partial R})^2 - \frac{10C_{10}R^{2m-1}\alpha_0 n(T-T_0)}{A^{2m}\varphi^6(R,T)} f(R,T)(1+\frac{\partial U}{\partial R})^2 \\ &+\frac{4mC_{01}R^{m-1}}{A^m\varphi^7(R,T)} f(R,T)(1+\frac{\partial U}{\partial R})^2(1+\frac{U}{R})^2 - \frac{28C_{01}R^{2m-1}\alpha_0 n(T-T_0)}{A^{2m}\varphi^8(R,T)} f(R,T)(1+\frac{\partial U}{\partial R})^2(1+\frac{U}{R})^2 \\ &+\frac{2}{R}((1+\frac{\partial U}{\partial R})^2 - (1+\frac{U}{R})^2)(\frac{2C_{10}R^m}{A^m\varphi^5(R,T)} f(R,T) + \frac{2C_{01}R^m}{A^m\varphi^7(R,T)} f(R,T)(1+\frac{U}{R})^2)\end{aligned} \tag{38}$$

2.3. Energy Equation

From the balance energy equation in the absence of heat energy generation, the total rate of heat energy may be found from [41]

$$\dot{Q} = -\nabla.q \tag{39}$$

where q represents the heat flux.

Here the steady-state heat conduction is considered. So, Eq. (39) can be rewritten as follows

$$\nabla.q = 0 \rightarrow q = -K(R,T)\nabla T \rightarrow \nabla.q = \nabla.(-K(R,T)\nabla T) = 0 \tag{40}$$

$$K\nabla^2 T + \nabla K.\nabla T = 0 \tag{41}$$

Due to the symmetry, the following identity holds in spherical coordinates:

$$\vec{\nabla} = \frac{\partial}{\partial R}\hat{e}_R \tag{42}$$

$$\nabla^2 f = (\frac{\partial^2}{\partial R^2} + \frac{2}{R}\frac{\partial}{\partial R})f \tag{43}$$

In spherical coordinate, the equation of heat conduction is:

$$K\frac{\partial T^2}{\partial R^2} + \frac{2K}{R}\frac{\partial T}{\partial R} + (\frac{\partial K}{\partial R})(\frac{\partial T}{\partial R}) = 0 \tag{44}$$

By considering $K(R) = K_0 f(T)(\frac{R}{A})^m$, the energy equation can be described:

$$\psi_6\frac{\partial T^2}{\partial R^2} + \psi_7\frac{\partial T}{\partial R} + \psi_8 = 0 \tag{45}$$

where

$$\psi_6 = 1 \tag{46}$$

$$\psi_7 = \frac{n+2}{R} \tag{47}$$

$$\psi_8 = \frac{a}{1+aT}(\frac{\partial T}{\partial R})^2 \tag{48}$$

2.4. Nonlinear finite element form of the governing equation

The coupled governing equations may be described as follows:

$$M\ddot{\phi} + C\dot{\phi} + K\phi = F \ , \ \phi = \begin{Bmatrix} U \\ T \end{Bmatrix} \tag{49}$$

The displacement and temperature are represented as follows:

$$U = [N(R)]\{U\} \ \ , \ T = [N(R)]\{T\} \tag{50}$$

Due to the nonlinear behavior of thermo-hyperelastic materials, it is acceptable to use high-order finite elements. So, the nonlinear shape functions are presented as [32]:

$$N_1 = -\frac{9}{16}(\xi+\frac{1}{3})(\xi-\frac{1}{3})(\xi+1) \tag{51}$$

$$N_2 = \frac{27}{16}(\xi+1)(\xi-\frac{1}{3})(\xi-1) \tag{52}$$

$$N_3 = -\frac{27}{16}(\xi+1)(\xi+\frac{1}{3})(\xi-1) \tag{53}$$

$$N_4 = \frac{9}{16}(\xi+\frac{1}{3})(\xi-\frac{1}{3})(\xi+1) \tag{54}$$

where ξ is the local coordinate and its values are between -1 and +1.

By using the Galerkin method, the nonlinear finite element equations can be derived.

By multiplying the differential equations (33) and (45) by $4\pi\int_0^l N^T R^2 dR$ and substituting Eqs. (50-54), we finally obtain the finite element model**:**

$$\begin{aligned} k_{11} &= -4\pi\int_0^l \psi_1 \frac{\partial N}{\partial R}\frac{\partial N^T}{\partial R}R^2 dR - 4\pi\int_0^l \frac{\partial \psi_1}{\partial R}N^T \frac{\partial N}{\partial R}R^2 dR - 8\pi\int_0^l \psi_1 N^T \frac{\partial N}{\partial R}R dR \\ &+4\pi\int_0^l \psi_2 N^T \frac{\partial N}{\partial R}R^2 dR + 4\pi\int_0^l \psi_4 N^T N R^2 dR \end{aligned} \tag{55}$$

$$k_{12} = 4\pi\int_0^l \psi_3 \frac{\partial N}{\partial R}N^T R^2 dR \tag{56}$$

$$k_{21} = 0 \tag{57}$$

$$k_{22} = -4\pi\int_0^l \frac{\partial N}{\partial R}\frac{\partial N^T}{\partial R}R^2 dR - 8\pi\int_0^l N^T \frac{\partial N}{\partial R}R dR + 4\pi\int_0^l \psi_7 N^T \frac{\partial N}{\partial R}R^2 dR \tag{58}$$

$$c_{11} = c_{12} = c_{21} = c_{22} = 0 \tag{59}$$

$$m_{11} = m_{12} = m_{21} = m_{22} = 0 \tag{60}$$

$$f_1 = -4\pi \int_0^l \psi_5 N^T R^2 dR \tag{61}$$

$$f_2 = -4\pi \int_0^l \psi_8 N^T R^2 dR \tag{62}$$

The stiffness matrix in Eq. (49) is dependent on the unknown displacement and temperature. So, Eq. (49) can be solved by using a suitable iterative approximation technique. Here, the Newton-Raphson method is used . The iterative solution may be ended when the following condition is happened:

$$\left| \frac{|\phi_{i+1}| - |\phi_i|}{|\phi_{i+1}|} \right| \leq 0.0001 \tag{63}$$

where j is the iteration counter.

3 RESULTS AND DISCUSSIONS

3.1. Verification of the results

In order to validate the calculation methodology as well as the accuracy of the results obtained, a comparision of the results obtained in this study and those found in the literature. The parameters of the material based on the Mooney-Rivlin model are listed in Table 1.[21]

Table 1 The parameters of the hyperelastic model [21]

$C_{10}(MPa)$	$C_{01}(MPa)$
0.162	5.9

In this section, we consider a thick sphere with the following characteristics: A=0.1 m, B=0.2 m. The applied internal and external pressures are Pi=0.5 Mpa and Po=0 Mpa, respectively.

The stress componenrts of the hyperelastic hollow sphere predicted by our formulation and Ref [21] are compared in Figs. 2 and 3, respectively. As it is observed, the results obtained with our formulation have considerable accuracy, as they are very close to the results obtained by Ref [21].

3.2. Parametric studies

Here, the influences of the constitutive, heterogeneity, temperature dependency, and loading parameters on the displacement, stresses, and temperature distribution are studied. In this research, a thermo-hyperelastic constitutive model is formulated for rubber that is in the incompressible material category. It should be noted that the physical

and thermophysical properties of the rubber-like hyperelastic material used in this investigation, belong to the category of FG materials with exponential function variation material used properties in the radial direction.

3.2.1. The influence of the constitutive parameters of the thermo hyperelastic material

Here, three distinct materials are considered to investigate the influence of the constitutive parameters of thermo hyperelastic on the displacement, stress, and temperature distribution of the FG hollow sphere. It is assumed that the inner and outer radius of the sphere are 3 mm and 8mm, respectively, and the internal pressure of the sphere is 1 MPa. The mechanical and thermal properties of the thermo hyperelastic model of the considered three materials are reported in Table 2.

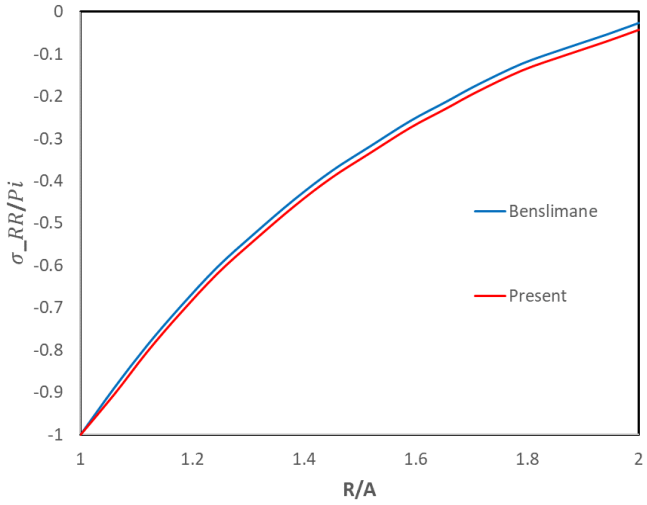

Fig. 2
A comparison between the present finite element formulation result and Ref [21] for the radial stress distribution through the thickness of the hyperelastic sphere.

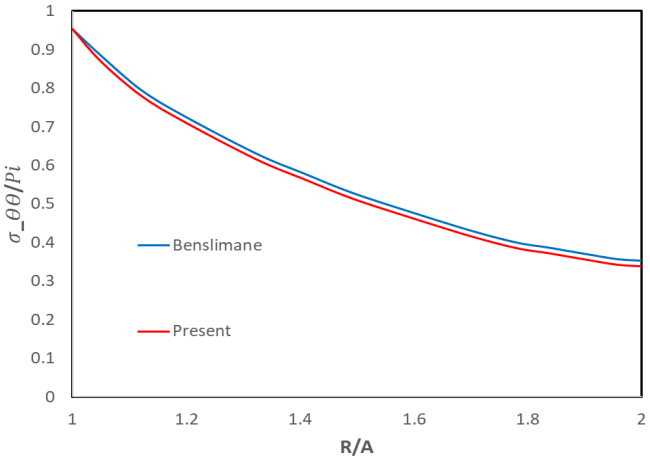

Fig. 3
A comparison between the present finite element formulation result and Ref [21] for the hoop stress distribution through the thickness of the hyperelastic sphere.

Table 2 The parameters of the Mooney-Rivlin model of the considered three different materials

Material	$C_{10}(MPa)$	$C_{01}(MPa)$	$K(W/mK)$	$\alpha(1/K)$	Reference
Silicon Rubber	0.200912	0.004235	1.9	286e-6	[42]
Vulcanized Rubber	0.390	0.015	0.15	225e-6	[43]
PVC	1.478	3.315	0.16	65.5e-6	[17]

According to Figure 4 and Table 2, the silicon rubber is softer than other thermo hyperelastic materials and its diformation because of an internal pressure of 1 MPa is about 1.86mm, indicates a large elongation. Also, it is clear that, PVC is the stiffest material. Material listed in Table 2 may be sorted in ascending order according to their rigidity as silicon rubber, vulcanized rubber and PVC, respectively.

Figures 5 and 6 show the distribution of radial and hoop stress through the thickness of different materials. According to these figures, radial and hoop stress are the smallest for PVC. In addition, PVC has a significant variation in the magnitudes of radial and hoop stress than the other materials.

For a homogeneous elastic pressure vessel whose magnitudes of the elastic modulus and Poisson's ratio quantities do not vary in radial direction , the radial distribution of the stress components are independent of material propereties. However, for a multi-layer composite vessel or a multi-layer vessel whose material properties vary from one layer to another, the distribution of the stress components vary in the radial direction. For a hyperelastic material, the slope of the stress-strain curve (i.e., the elastic modulus) is load-dependent and is not independent of the magnitude of the induced stress. Therefore, the apparently single-layer hyperelastic vessel may be assumed to be constructed from infinte sub-layer whose elastic moduli are not only different but also dependent on the imposed stresses. It is evident that the entire distribution of the mentioned elastic moduli becomes quite different for a different hyperelastic material. Therefore, distribution of the stress components are material-dependent in hyperelastic vessels.

The distribution of the temperature through the thickness is indicated in Figure 7. It is clear that the temperature in vulcanized rubber is the highest and silicon rubber has the lowest one. Also, the variation of the temperature in vulcanized rubber is considerable.

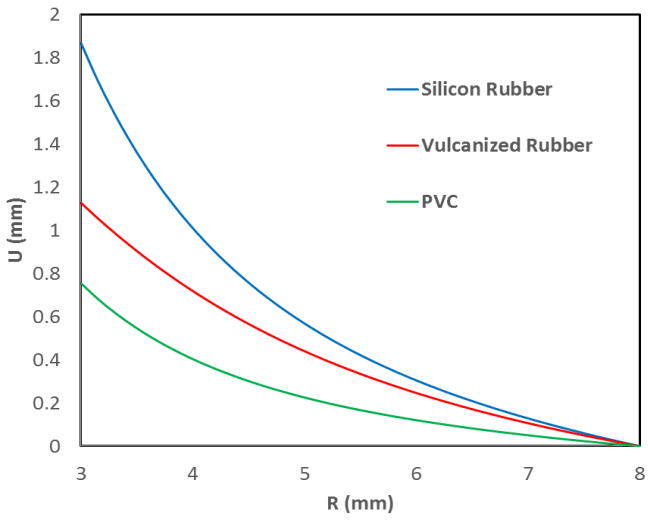

Fig. 4
The through-thickness distribution of the displacement of the hollow sphere for different materials.

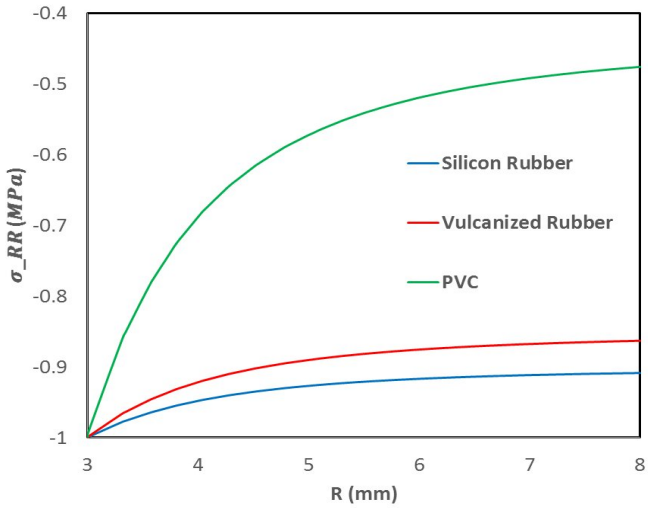

Fig. 5
The through-thickness distribution of the radial stress of the hollow sphere for different materials.

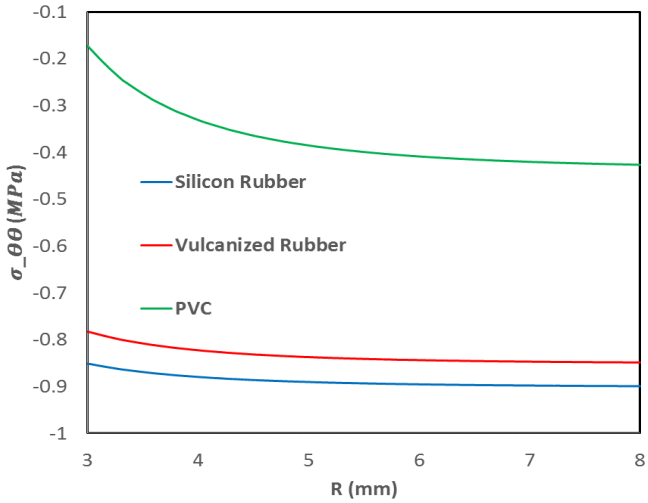

Fig. 6
The through-thickness distribution of the hoop stress of the hollow sphere for different materials.

3.2.2. The effects of the internal pressure

In this section, displacement, stress components, and temperature distribution through the thickness are plotted for various internal pressures to analyse the influence of the internal pressure on the responses of the hollow FG thermo hyperelastic sphere. It is assumed that the sphere is made of PVC. Table 2, listed the mechanical and thermal paroperties of the material . Here, the internal pressures are from 1 to 5MPa.

Figures (8-11) show that if the internal pressure increases, the effect of the constitutive and kinematic nonlinearities on the resultant deformation and stress components will be more remarkable. Also, by increasing the internal pressure, the displacement, stresses, and temperature increase. In addition, if the internal pressure increases, the variations of displacement, stress components, and temperature will be more sighnificant in the vicinity of the interior boundary.

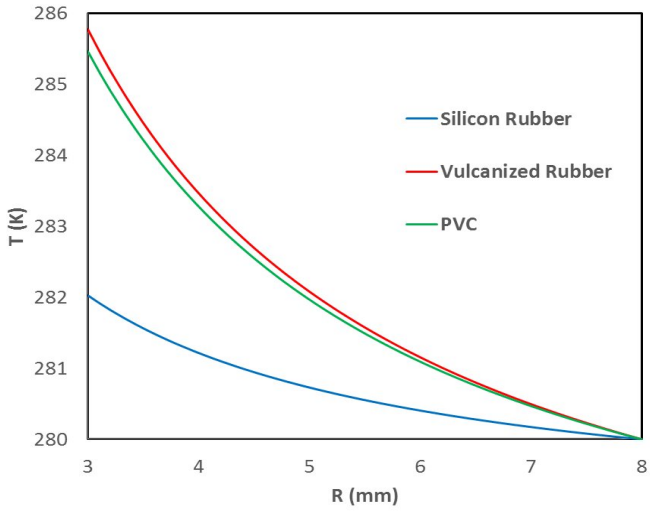

Fig. 7
The through-thickness distribution of the temperature of the hollow sphere for different materials.

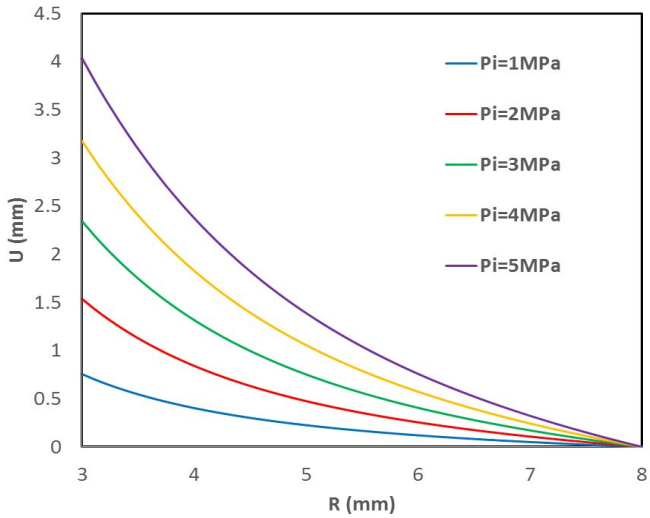

Fig. 8
The through-thickness distribution of the displacement of the hollow sphere for different internal pressures.

3.2.3. The influence of the temperature-dependency of the thermo-hyperelastic material

Figures 12-15 indicate the effect of the temperature dependency of the thermo-hyperelastic material on the distributions of deformation, stress components, and temperature through the thickness. According to Figure 12, the radial displacement decreases through the thickness of the hollow sphere. Also, The radial displacement is maximum at the interior boundary and is zero at the exterior surface. Also, the radial displacement decreases by increasing the temperature dependency parameter (a) for different radius of sphere.

The distribution of radial stress through the thickness is shown in Figure 13 for various values of the temperature-dependency parameter. The magnitude of radial stress decreases through the thickness. In addition, if the temperature dependency parameter (a) increses, the radial stress decreases in different radius of sphere. Also, at points far from the inner boundary, the radial stress indicates considerable variances for varioud values of (a).

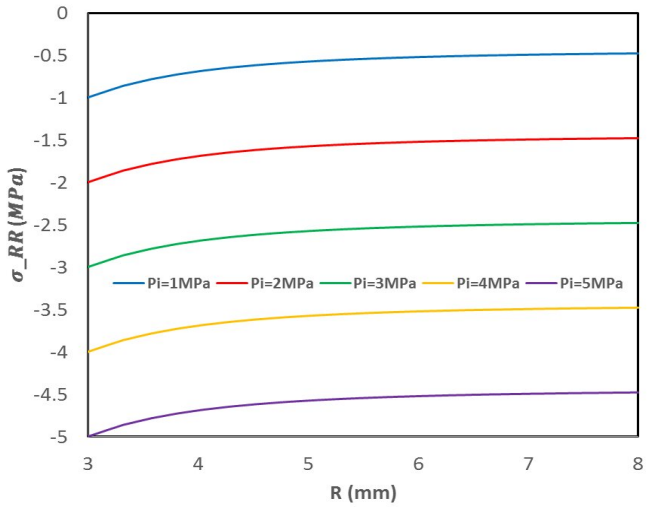

Fig. 9
The through-thickness distribution of the radial stress of the hollow sphere for different internal pressures.

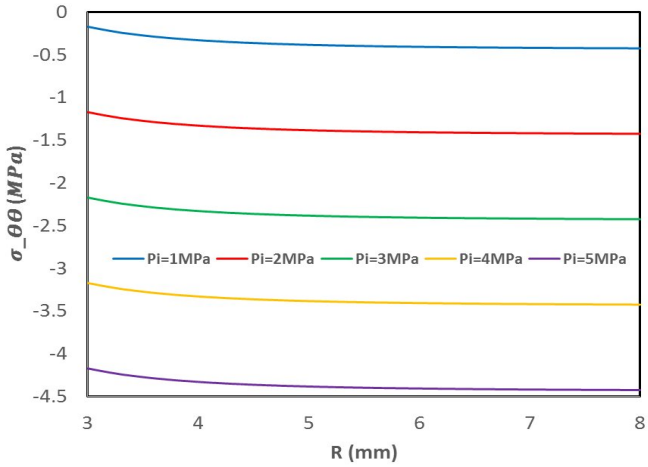

Fig. 10
The through-thickness distribution of the hoop stress of the hollow sphere for different internal pressures.

Figure 14 shows the effect of the temperature-dependency parameter on the distribution of hoop stress. According to this figure, the hoop stress rises through the thickness. In addition, if the temperature dependency parameter (a) increses,the hoop stress reduces in each arbitrary radius.

The distribution of temperature through the thickness is plotted in Figure 15. This figure shows that the value of temperature decreases through the thickness. Also, by rising the value of the temperature-dependency parameter, the magnitude of temperature decreases. It is clear that, the temperature dependency of the material has not sighnificant effect on the distribution of temperature.

3.2.4. The effects of the heterogeneity of the material

Figures 16-19 show the distribution of displacement, stress components, and temperature through the thickness of the hollow sphere for various material parameters (m). According to Figure 16, in the interior boundary, the radial displacement is maximum and it reduces through the thickness.Also, it is zero in the exterior boundary because the

exterior boundary is fixed. Moreover, the radial displacement in different radiu of sphere reduces by rising the material parameter (m). This distribution occurs because of increasing material strength by increasing (m).

Figure 17 shows the variation of radial stress for various values of material parameters (m). According to this figure, at first, the radial stress in different radius of sphere, reduces by rising (m) and then increases. Also, at points far from the inner boundary, the radial stress indicates considerable differences for different m.

The variation of hoop stress is shown in Figure 18 for different values of material parameter (m). In contrast with radial stress which has the same distribution for different (m), the most interesting part of the results is distribution of hoop stress which changing from monotonically increasing in R to monotonically decreasing in R as a function of gradient parameter (m). This variation is very valuable for the design of hollow spheres to delay or avoid failure.

Figure 19 shows the variation of temperature for different values of material parameter m. According to this figure by increasing the value of material parameter in an arbitrary radius, the magnitude of temperature decreases. Moreover, the maximum value of temperature takes place at the inner boundary of the sphere and reaches 280 K at the outer surface satisfying the boundary condition.

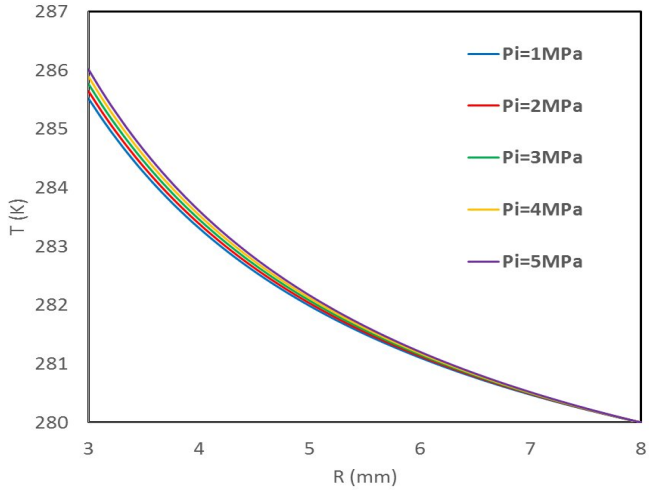

Fig. 11
The through-thickness distribution of the temperature of the hollow sphere for different internal pressures.

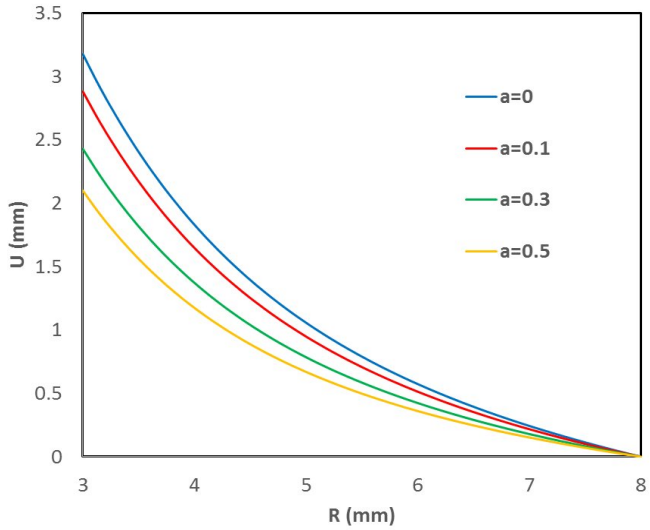

Fig. 12
The through-thickness distribution of the displacement of the hollow sphere for different temperature-dependency parameters.

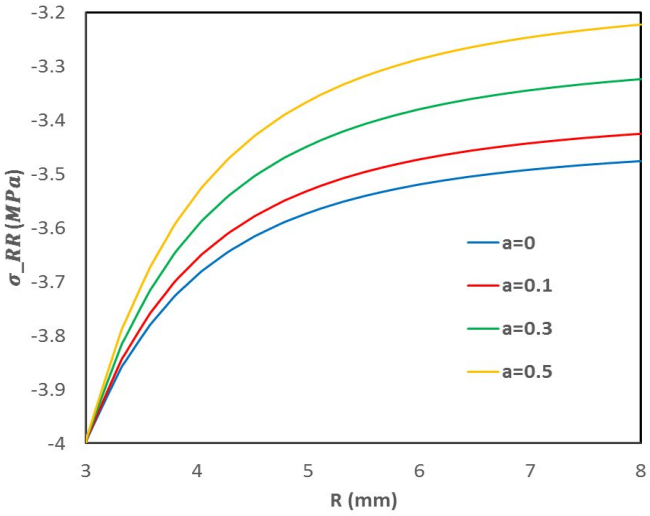

Fig. 13
The through-thickness distribution of the radial stress of the hollow sphere for different temperature dependency parameter.

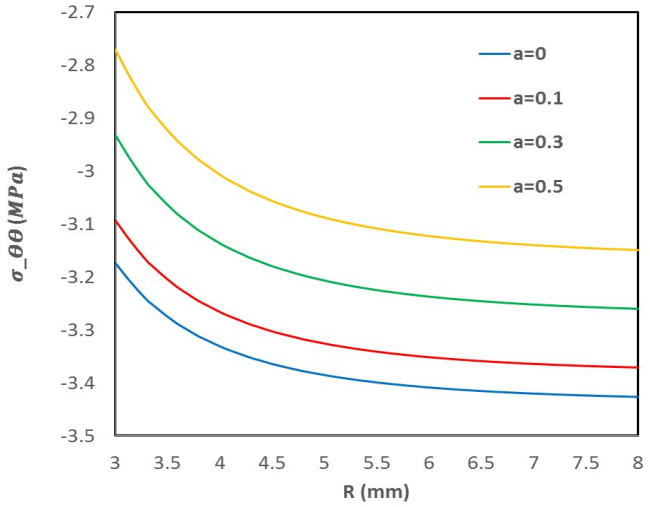

Fig. 14
The through-thickness distribution of the hoop stress of the hollow sphere for different temperature dependency parameters.

4 CONCLUSIONS

Here, a nonlinear finite element formulation is developed for deformation, stress, and thermal analyses of functionally graded thermo hyperelastic hollow spheres with temperature-dependent material. Mooney-Rivlin strain energy function is used to model hyperelastic behavior. It is assumed that the material parameter changes in radial direction continuously according to a power law. By applying the internal pressure and thermal boundary conditions, displacement, stress components, and temperature distribution are developed for a hollow thermo hyperelastic sphere. To show the effect of constitutive parameters on the distribution of deformation, radial/hoop stresses, and temperature, three hyperelastic materials such as silicon rubber, vulcanized rubber, and PVC are considered. In addition, the influence of the temperature-dependency of thermo-hyperelastic material and inhomogeneity is shown by considering the different values of temperature dependency parameter (a) and material inhomogeneity parameters (m). Also, the variation of displacement, radial/ hoop stresses, and temperature are shown for various values of

internal pressures. Here, the internal pressure and thermal boundary conditions applied to the FG thermo hyperelastic sphere and it is realized that the magnitude of displacement, stress components, and temperature increases by rising the values of interior pressure. Also, by increasing temperature dependency parameter (a), displacement, stress component, and temperature decrease. In addition, by rising the inhomogeneity of the material (m), in each different radius of sphere, radial deformation decreases while the magnitude of radial stress increases. The above-presented results show that the constitutive parameter, temperature dependency of material, and inhomogeneity parameter have a remarkable effect on the mechanical and thermal behavior of thick hollow FG thermo hyperelastic sphere. Thus by choosing a proper hyperelastic material, inhomogeneity (m), and temperature dependency parameter (a), engineers will design a precise thermo hyperelastic sphere for some important requirements.

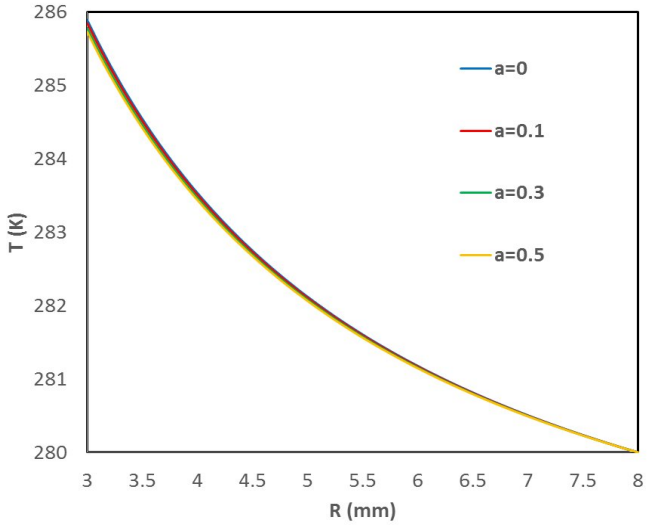

Fig. 15
The through-thickness distribution of the temperature of the hollow sphere for different temperature dependency parameters.

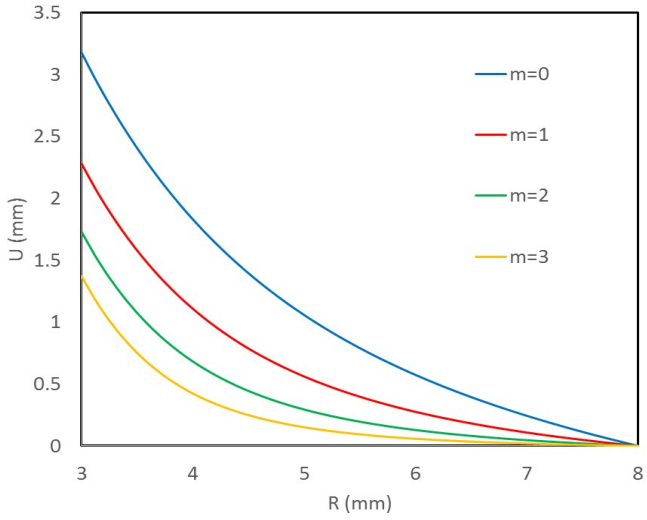

Fig. 16
The through-thickness distribution of the displacement of the hollow sphere for different heterogeneity parameters.

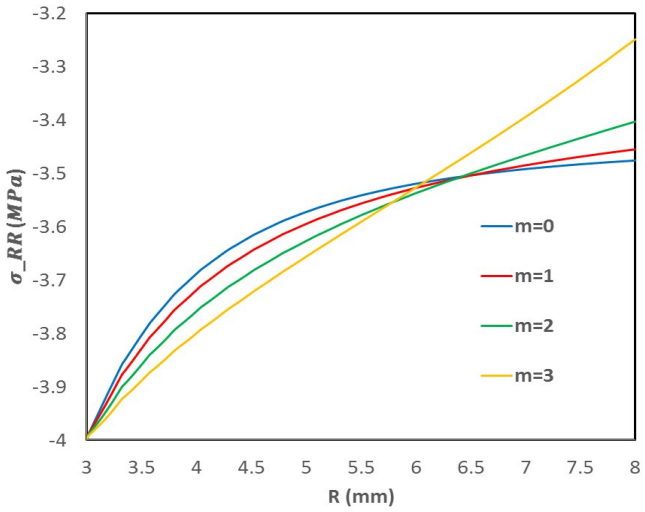

Fig. 17
The through-thickness distribution of the radial stress of the hollow sphere for different heterogeneity parameters.

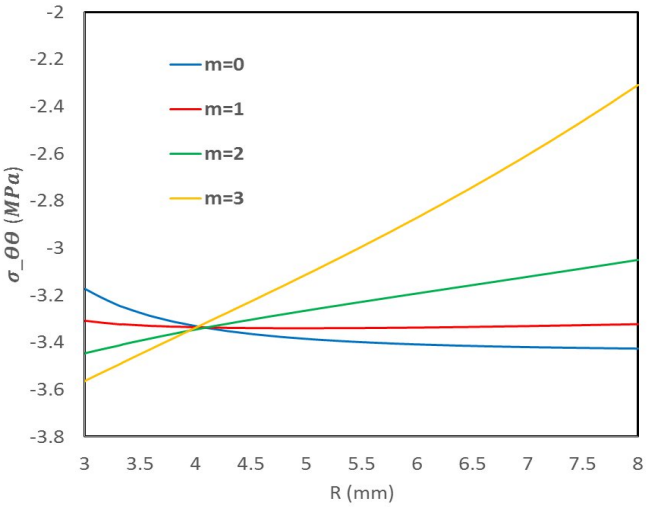

Fig. 18
The through-thickness distribution of the hoop stress of the hollow sphere for different heterogeneity parameters.

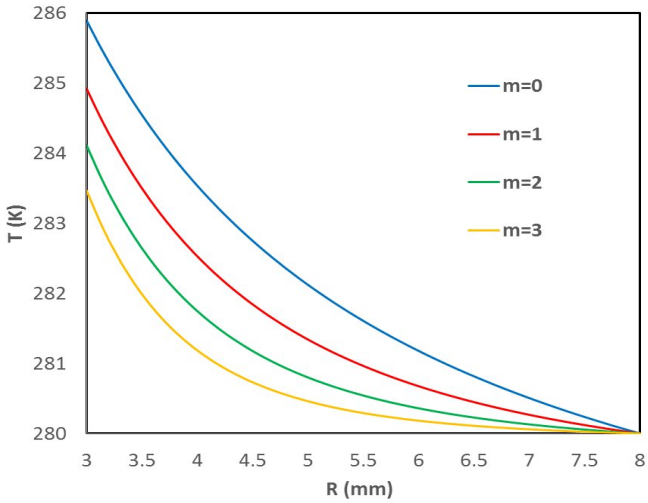

Fig. 19
The through-thickness distribution of the temperature of the hollow sphere for different heterogeneity parameters.

5 NOMENCLATURE

C_{10}, C_{10}	Mooney Rivlin coefficents
E	Green's strain tensor
F	Deformation gradient
h	Heat transfer coefficient
I_C, II_C, III_C	Right Cauchy-Green tensor invariants
J	Jacobian
K	Thermal conductivity
$N_i(R)$	Shape functions
q	Heat flux
T	Temperature
T_0	Reference temperature
U	Displacement vector
R	Reference coordinate
α	Thermal expansion coefiicient
ψ	Strain energy function
γ	Second Piola-Kirchhoff stress
σ	Traction
ρ	Density

REFERENCES

[1] B. Kim, S. B. Lee, J. Lee, S. Cho, H. Park, S. Yeom, S. H. Park, A comparison among Neo-Hookean model, Mooney-Rivlin model, and Ogden model for chloroprene rubber, *International Journal of Precision Engineering and Manufacturing,* Vol. 13, pp. 759-764, 2012.

[2] M. Mooney, A theory of large elastic deformation, *Journal of applied physics,* Vol. 11, No. 9, pp. 582-592, 1940.

[3] R. W. Ogden, Large deformation isotropic elasticity–on the correlation of theory and experiment for incompressible rubberlike solids, *Proceedings of the Royal Society of London. A. Mathematical and Physical Sciences,* Vol. 326, No. 1567, pp. 565-584, 1972.

[4] D. Taghizadeh, A. Bagheri, H. Darijani, On the hyperelastic pressurized thick-walled spherical shells and cylindrical tubes using the analytical closed-form solutions, *International Journal of Applied Mechanics,* Vol. 7, No. 02, pp. 1550027, 2015.

[5] D. Aranda-Iglesias, G. Vadillo, J. A. Rodríguez-Martínez, Constitutive sensitivity of the oscillatory behaviour of hyperelastic cylindrical shells, *Journal of Sound and Vibration,* Vol. 358, pp. 199-216, 2015.
[6] I. D. Breslavsky, M. Amabili, M. Legrand, Static and dynamic behavior of circular cylindrical shell made of hyperelastic arterial material, *Journal of Applied Mechanics,* Vol. 83, No. 5, pp. 051002, 2016.
[7] Y. Anani, G. H. Rahimi, Stress analysis of rotating cylindrical shell composed of functionally graded incompressible hyperelastic materials, *International Journal of Mechanical Sciences,* Vol. 108, pp. 122-128, 2016.
[8] A. Ghorbanpour Arani, E. Haghparast, A. Ghorbanpour Arani, Size-dependent vibration of double-bonded carbon nanotube-reinforced composite microtubes conveying fluid under longitudinal magnetic field, *Polymer Composites,* Vol. 37, No. 5, pp. 1375-1383, 2016.
[9] A. Ghorbanpour-Arani, A. Rastgoo, M. Sharafi, R. Kolahchi, A. Ghorbanpour Arani, Nonlocal viscoelasticity based vibration of double viscoelastic piezoelectric nanobeam systems, *Meccanica,* Vol. 51, pp. 25-40, 2016.
[10] A. Ghorbanpour Arani, M. Jamali, A. Ghorbanpour-Arani, R. Kolahchi, M. Mosayyebi, Electro-magneto wave propagation analysis of viscoelastic sandwich nanoplates considering surface effects, *Proceedings of the Institution of Mechanical Engineers, Part C: Journal of Mechanical Engineering Science,* Vol. 231, No. 2, pp. 387-403, 2017.
[11] A. Ghorbanpour-Arani, A. Rastgoo, A. Hafizi Bidgoli, R. Kolahchi, A. Ghorbanpour Arani, Wave propagation of coupled double-DWBNNTs conveying fluid-systems using different nonlocal surface piezoelasticity theories, *Mechanics of Advanced Materials and Structures,* Vol. 24, No. 14, pp. 1159-1179, 2017.
[12] K. Narooei, M. Arman, Modification of exponential based hyperelastic strain energy to consider free stress initial configuration and Constitutive modeling, *Journal of Computational Applied Mechanics,* Vol. 49, No. 1, pp. 189-196, 2018.
[13] A. Ataee, R. Noroozi, Behavioral optimization of pseudo-neutral hole in hyperelastic membranes using functionally graded cables, *Journal of Computational Applied Mechanics,* Vol. 49, No. 2, pp. 282-291, 2018.
[14] H. Gharooni, M. Ghannad, Nonlinear analytical solution of nearly incompressible hyperelastic cylinder with variable thickness under non-uniform pressure by perturbation technique, *Journal of Computational Applied Mechanics,* Vol. 50, No. 2, pp. 395-412, 2019.
[15] H. Gharooni, M. Ghannad, Nonlinear analysis of radially functionally graded hyperelastic cylindrical shells with axially-varying thickness and non-uniform pressure loads based on perturbation theory, *Journal of Computational Applied Mechanics,* Vol. 50, No. 2, pp. 324-340, 2019.
[16] Y. Anani, G. Rahimi, On the stability of internally pressurized thick-walled spherical and cylindrical shells made of functionally graded incompressible hyperelastic material, *Latin American Journal of Solids and Structures,* Vol. 15, pp. e37, 2018.
[17] M. Shariyat, M. Khosravi, M. Y. Ariatapeh, M. Najafipour, Nonlinear stress and deformation analysis of pressurized thick-walled hyperelastic cylinders with experimental verifications and material identifications, *International Journal of Pressure Vessels and Piping,* Vol. 188, pp. 104211, 2020.
[18] Z. Zhao, D. Niu, H. Zhang, X. Yuan, Nonlinear dynamics of loaded visco-hyperelastic spherical shells, *Nonlinear Dynamics,* Vol. 101, pp. 911-933, 2020.
[19] A. Ghorbanpour-Arani, M. Abdollahian, A. Ghorbanpour Arani, Nonlinear dynamic analysis of temperature-dependent functionally graded magnetostrictive sandwich nanobeams using different beam theories, *Journal of the Brazilian Society of Mechanical Sciences and Engineering,* Vol. 42, pp. 1-20, 2020.
[20] E. Haghparast, A. Ghorbanpour-Arani, A. G. Arani, Effect of fluid–structure interaction on vibration of moving sandwich plate with Balsa wood core and nanocomposite face sheets, *International Journal of Applied Mechanics,* Vol. 12, No. 07, pp. 2050078, 2020.
[21] A. Benslimane, Nonlinear stress analysis of rubber-like thick-walled sphere using different constitutive models, *Materials Today: Proceedings,* Vol. 53, pp. 46-51, 2022.
[22] S. Jemioło, A. Franus, Finite Element Method Modelling of Long and Short Hyperelastic Cylindrical Tubes, in *Proceeding of,* Springer, pp. 152-160.
[23] F. Aghaienezhad, R. Ansari, M. Darvizeh, On the stability of hyperelastic spherical and cylindrical shells subjected to external pressure using a numerical approach, *International Journal of Applied Mechanics,* Vol. 14, No. 10, pp. 2250094, 2022.
[24] A. Anssari-Benam, A. Bucchi, G. Saccomandi, Modelling the inflation and elastic instabilities of rubber-like spherical and cylindrical shells using a new generalised neo-Hookean strain energy function, *Journal of Elasticity,* Vol. 151, No. 1, pp. 15-45, 2022.
[25] A. A. Ghorbanpour-Arani, Z. Khoddami Maraghi, A. Ghorbanpour Arani, The frequency response of intelligent composite sandwich plate under biaxial in-plane forces, *Journal of Solid Mechanics,* Vol. 15, No. 1, pp. 1-18, 2023.
[26] A. Ghorbanpour Arani, N. Miralaei, A. Farazin, M. Mohammadimehr, An extensive review of the repair behavior of smart self-healing polymer matrix composites, *Journal of Materials Research,* Vol. 38, No. 3, pp. 617-632, 2023.
[27] P. Sourani, A. Ghorbanpour Arani, M. Hashemian, S. Niknejad, Nonlinear dynamic stability analysis of CNTs reinforced piezoelectric viscoelastic composite nano/micro plate under multiple physical fields resting on smart foundation, *Proceedings of the Institution of Mechanical Engineers, Part C: Journal of Mechanical Engineering Science,* Vol. 238, No. 10, pp. 4307-4342, 2024.
[28] Z. Yosibash, D. Weiss, S. Hartmann, High-order FEMs for thermo-hyperelasticity at finite strains, *Computers & Mathematics with Applications,* Vol. 67, No. 3, pp. 477-496, 2014.

[29] A. Almasi, M. Baghani, A. Moallemi, Thermomechanical analysis of hyperelastic thick-walled cylindrical pressure vessels, analytical solutions and FEM, *International Journal of Mechanical Sciences,* Vol. 130, pp. 426-436, 2017.
[30] J. Xu, X. Yuan, H. Zhang, Z. Zhao, W. Zhao, Combined effects of axial load and temperature on finite deformation of incompressible thermo-hyperelastic cylinder, *Applied Mathematics and Mechanics,* Vol. 40, No. 4, pp. 499-514, 2019.
[31] J. Xu, X. Yuan, H. Zhang, F. Zheng, L. Chen, Nonlinear vibrations of thermo-hyperelastic moderately thick cylindrical shells with 2: 1 internal resonance, *International Journal of Structural Stability and Dynamics,* Vol. 20, No. 05, pp. 2050067, 2020.
[32] M. Mirparizi, A. Fotuhi, Nonlinear coupled thermo-hyperelasticity analysis of thermal and mechanical wave propagation in a finite domain, *Physica A: Statistical Mechanics and its Applications,* Vol. 537, pp. 122755, 2020.
[33] F. Shakeriaski, M. Ghodrat, J. Escobedo-Diaz, M. Behnia, The nonlinear thermo-hyperelasticity wave propagation analysis of near-incompressible functionally graded medium under mechanical and thermal loadings, *Archive of Applied Mechanics,* Vol. 91, No. 7, pp. 3075-3094, 2021.
[34] R. Wang, H. Ding, X. Yuan, N. Lv, L. Chen, Nonlinear singular traveling waves in a slightly compressible thermo-hyperelastic cylindrical shell, *Nonlinear Dynamics*, pp. 1-15, 2022.
[35] A. Bakhtiyari, M. Baniasadi, M. Baghani, A modified constitutive model for shape memory polymers based on nonlinear thermo-visco-hyperelasticity with application to multi-physics problems, *International Journal of Applied Mechanics,* Vol. 15, No. 04, pp. 2350032, 2023.
[36] V. Mohammadlou, Z. Khoddami Maraghi, A. Ghorbanpour Arani, Thermoelastic analysis of axisymmetric conical shells: Investigating stress–strain response under uniform heat flow with semi-coupled approach, *Numerical Heat Transfer, Part A: Applications*, pp. 1-22, 2024.
[37] T. Netz, S. Hartmann, A monolithic finite element approach using high-order schemes in time and space applied to finite strain thermo-viscoelasticity, *Computers & Mathematics with Applications,* Vol. 70, No. 7, pp. 1457-1480, 2015.
[38] S. Lu, K. Pister, Decomposition of deformation and representation of the free energy function for isotropic thermoelastic solids, *International Journal of Solids and Structures,* Vol. 11, No. 7-8, pp. 927-934, 1975.
[39] W. Ehlers, G. Eipper, The simple tension problem at large volumetric strains computed from finite hyperelastic material laws, *Acta Mechanica,* Vol. 130, No. 1-2, pp. 17-27, 1998.
[40] B. Liu, X. Guo, G. Qi, D. Zhang, Quality evaluation of rubber-to-metal bonded structures based on shearography, *Science China Physics, Mechanics & Astronomy,* Vol. 58, pp. 1-8, 2015.
[41] M. Homayouni, M. Shariyat, O. Rahmani, Thermally nonlinear generalized thermoelasticity investigation of a functionally graded thick hollow cylinder based on the finite difference method, *Thin-Walled Structures,* Vol. 177, pp. 109359, 2022.
[42] M. Shojaeifard, K. Wang, M. Baghani, Large deformation of hyperelastic thick-walled vessels under combined extension-torsion-pressure: analytical solution and FEM, *Mechanics Based Design of Structures and Machines,* Vol. 50, No. 12, pp. 4139-4156, 2022.
[43] A. F. Bower, 2009, *Applied mechanics of solids*, CRC press,